NMR for Equilateral Triangular Geometry under Conditions of Surface Relaxivity - Analytical and Random Walk Solution

J. Finjord [a] A. Hiorth [b,*] U. H. a Lad [a] S. M. Skjæveland [a]

[a] *University of Stavanger, N-4036 Stavanger,Norway*

[b] *RF-Rogaland Research, P. O. Box 8046, N-4068 Stavanger, Norway*

Abstract

We consider analytical and numerical solution of NMR relaxation under the condition of surface relaxation in an equilateral triangular geometry. We present an analytical expression for the Green's function in this geometry. We calculate the transverse magnetic response for the CPMG sequence, single-phase, both analytically and numerically. There is a very good match between the analytical and numerical results.

Key words: CPMG NMR, diffusion, equilateral triangle, random walk, analytical
PACS: 76.60, 31.70, 33.25

1 Introduction

In the oil industry there has been a great interest in using NMR as a tool for improved reservoir characterizing. NMR can be used as an in situ tool for measuring oil and brine content in saturated porous rocks[1,2,3,4]. The wetting state of a porous rock is a parameter of great importance in oil recovery. Wettability is the ability of a phase to adhere to the surface of the rock. NMR is a very promising tool in order to obtain in situ information about wettability. Wettability is related to the enhanced relaxation felt by the confined spins. This effect was first considered in the classical papers by Brownstein and Tarr by studying classical diffusion [5,6]. For a completely water wet rock, saturated with oil and water, only the water phase will experience enhanced

* Corresponding author
Email address: ah@rf.no (A. Hiorth).

surface relaxation. If oil enters a porous rock, initially water filled and water wet, the oil can change the wetting state of the rock from water-wet to more oil-wet. Surface active components in the oil can adsorb on the rock phase and change the wettability. The change of surface properties of the rock will produce a measurable effect on the NMR signal, this has been studied in numerous publications, see [7] and the references therein. Experiments on porous rocks is well suited for showing an effect of enhanced surface relaxation due to wettability change. However, by studying more simple systems, more information can be gained in order to understand how wettability will affect the magnetic signal. For this purpose an equilateral triangular geometry is well suited. This is because two or more phases can form a stable configuration inside the triangle. A great deal of attention have been devoted to triangles in order to understand the multi phase behavior of porous rocks[8,9,10]. Triangles are the basic building blocks in pore network models[11] and also bundle of equilateral triangular tubes models have been studied extensively [12,13]. Attempt of using a bundle of equilateral triangular tubes in interpreting NMR signal from porous rocks have also been done[14].

Experiments on triangular tubes single-phase and two-phase are in progress at our group. In order to interpret experiments properly one needs a good theoretical understanding of the magnetic response from equilateral tubes. In this paper we will present an analytical solution and a numerical (random walk) solution for the CPMG[15] sequence in an equilateral triangular geometry. Calculations and simulations for the PFGSE sequence[16,17,18], will be presented in a forthcoming paper.

2 Theory

The equilateral triangular geometry is a true two dimensional system, contrary to plate, cylinder and sphere geometry, first considered by Brownstein and Tarr[6]. This problem is much harder to solve, the technical reason for this is that it is not possible to choose a coordinate system where the axes are parallel to the sides of the triangle. Fortunately the calculation greatly simplifies because of a series of recent papers by Mccartin, which solves the diffusion equation in an equilateral triangular geometry[19,20,21]. The magnetization as a function of time is given by the following equations[5,6]:

$$\frac{\partial M(\mathbf{r},t)}{\partial t} = D\nabla^2 M(\mathbf{r},t) - \frac{M(\mathbf{r},t)}{T_{2b}}\,. \tag{1}$$

T_{2b} is the bulk relaxation and D the diffusion constant. At the surface, Σ, we have we have the following boundary condition:

$$D\hat{\mathbf{n}} \cdot \nabla M(\mathbf{r},t) + \rho M(\mathbf{r},t)|_{\mathbf{r}=\Sigma} = 0\,, \tag{2}$$

where $\hat{\mathbf{n}}$ is the outward normal and ρ the surface relaxivity. The magnetization of the sample is :

$$M(t) = \int_{\Delta} d\mathbf{r} M(\mathbf{r},t)\,, \tag{3}$$

where the integral is taken over the triangular domain. By introducing the Green's function we can write the magnetization as:

$$M(\mathbf{r},t) = e^{-t/T_{2b}} \int_{\Delta} d\mathbf{r}'\, \rho(\mathbf{r}') G(\mathbf{r}'|\mathbf{r};t)\,, \tag{4}$$

where $\rho(\mathbf{r}')$ is the initial spin density. $G(\mathbf{r}'|\mathbf{r};t)$ is the Green's function or the propagator. It is defined as the probability for a particle at position $\mathbf{r}'$ at time 0 to diffuse to point $\mathbf{r}$ during a time t. The propagator satisfies the diffusion equation at the interior of the pore space:

$$\frac{\partial G(\mathbf{r}|\mathbf{r}';t)}{\partial t} - D\nabla^2 G(\mathbf{r}|\mathbf{r}';t) = 0 \;\text{ and }\; G(\mathbf{r}|\mathbf{r}';t)|_{t=0} = \delta(\mathbf{r}-\mathbf{r}')\,, \tag{5}$$

where D is the diffusion constant. The boundary condition at the surface Σ :

$$D\hat{\mathbf{n}} \cdot \nabla G(\mathbf{r}|\mathbf{r}';t) + \rho\, G(\mathbf{r}|\mathbf{r}';t)|_{\mathbf{r}=\Sigma} = 0\,. \tag{6}$$

3 The Green's function in an equilateral triangular geometry

By using the standard eigenfunction expansion of the propagator:

$$G(\mathbf{r}|\mathbf{r}';t) = \sum_{i=0}^{\infty} \phi_i(\mathbf{r})\phi_i(\mathbf{r}') e^{-t/T_i}\,, \tag{7}$$

where $\{\phi_i\}$ are an orthonormal set of eigenfunctions with corresponding eigenvalues T_i. From equation (5) and (6) it then follows:

$$D\nabla^2\phi_i(\mathbf{r}) = -\frac{1}{T_i}\phi_i(\mathbf{r}) \;\text{ and }\; D\hat{\mathbf{n}} \cdot \nabla\phi_i(\mathbf{r}) + \rho\,\phi(\mathbf{r})|_{\mathbf{r}=\Sigma} = 0\,. \tag{8}$$

This equation needs to be solved in an equilateral triangle, shown in figure 1.The solution is in terms of *unnormalized* eigenfunctions[21] :

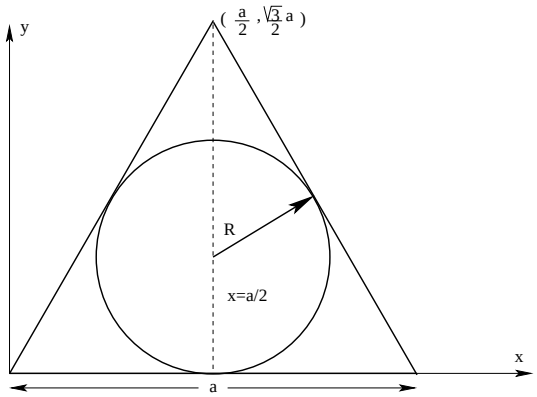

Fig. 1. Equilateral triangle of side length a and inscribed radius R

$$
\begin{aligned}
T^s_{ij}(x,y) &= \cos\left[\frac{\pi\lambda}{3R}(3R-y)-\delta_1\right]\,\cos\left[\frac{\sqrt{3}\pi(\mu-\nu)}{9R}(x-\sqrt{3}R)\right] \\
&+\cos\left[\frac{\pi\mu}{3R}(3R-y)-\delta_2\right]\,\cos\left[\frac{\sqrt{3}\pi(\nu-\lambda)}{9R}(x-\sqrt{3}R)\right] \\
&+\cos\left[\frac{\pi\nu}{3R}(3R-y)-\delta_3\right]\,\cos\left[\frac{\sqrt{3}\pi(\lambda-\mu)}{9R}(x-\sqrt{3}R)\right] \qquad (9) \\
T^a_{ij}(x,y) &= \cos\left[\frac{\pi\lambda}{3R}(3R-y)-\delta_1\right]\,\sin\left[\frac{\sqrt{3}\pi(\mu-\nu)}{9R}(x-\sqrt{3}R)\right] \\
&+\cos\left[\frac{\pi\mu}{3R}(3R-y)-\delta_2\right]\,\sin\left[\frac{\sqrt{3}\pi(\nu-\lambda)}{9R}(x-\sqrt{3}R)\right] \\
&+\cos\left[\frac{\pi\nu}{3R}(3R-y)-\delta_3\right]\,\sin\left[\frac{\sqrt{3}\pi(\lambda-\mu)}{9R}(x-\sqrt{3}R)\right]\,. \qquad (10)
\end{aligned}
$$

$R = a/(2\sqrt{3})$ is the radius of the inscribed circle in an equilateral triangle of side a. The index s, a of the eigenfunctions refers to symmetric,antisymmetric about the line $x = a/2$, respectively. The constants $\mu, \nu, \lambda, \delta_1, \delta_2, \delta_3$ are determined by solving the following three transcendental equations originating from the boundary condition (8):

$$
\begin{aligned}
[2L-M-N-(i+j)\pi]\tan L &= 3\gamma\,,\ -\frac{\pi}{2} < L \le 0 \\
[2M-N-L-i\pi]\tan M &= 3\gamma \quad ,\ 0 < M \le \frac{\pi}{2} \\
[2N-L-M-j\pi]\tan N &= 3\gamma \quad ,\ 0 < N \le \frac{\pi}{2}\,, \qquad (11)
\end{aligned}
$$

where $\gamma = R\rho/D$, $i = 0, 1, \ldots$, $j = i, i+1, \ldots$ and

$$
\begin{aligned}
&\delta_1 = L-M-N\ ,\ \delta_2 = -L+M-N\ ,\ \delta_3 = -L-M+N \\
&\mu = \frac{2M-N-L}{\pi} + i\ ,\ \nu = \frac{2N-L-M}{\pi} + j\ ,\ \lambda = -\mu-\nu\,. \qquad (12)
\end{aligned}
$$

Finally, the eigenvalues are given by:

$$T_{ij}^{-1} = \frac{2D}{27}\left(\frac{\pi}{R}\right)^2\left[\lambda^2+\mu^2+\nu^2\right]. \tag{13}$$

When $i=j$ we have $M=N$, $\delta_2=\delta_3$, $\mu=\nu$ and $2\pi\mu = \delta_2-\delta_1+2i\pi$. The eigenfunctions simplifies:

$$\begin{aligned} T_{ii}^s(x,y) &= \cos\left[\frac{2\pi\mu}{3R}y-\delta_2\right] \\ &\quad +2\cos\left[\frac{\pi\mu}{\sqrt{3}R}(\sqrt{3}R-x)\right]\cos\left[\frac{\pi\mu}{3R}(y-3R)+\delta_2\right] \\ T_{ii}^a(x,y) &= 0 \\ T_{ii}^{-1} &= \frac{4D}{9}\left(\frac{\pi\mu}{R}\right)^2. \end{aligned} \tag{14}$$

The complete set of orthogonal eigenfunctions is then $\{T_{ij}^s(i\geq j);\, T_{ij}^a(i>j)\}$, for further details on this point see[21].

In order to obtain explicit expressions for the propagator we need to normalize the eigenfunctions over the triangular domain i.e. :

$$N^{s,a2} = \int_0^{3R}\int_{y/\sqrt{3}}^{-y/\sqrt{3}+2\sqrt{3}R} T_{s,a}(x,y)T_{s,a}(x,y) \tag{15}$$

in an obvious notation, the subscript i,j has been suppressed. After a rather lengthy manipulation, the result can be written:

$$\begin{aligned} N^{s2} = -\frac{9\sqrt{3}R^2}{16\mu^2\pi^2}\Big\{ &-8-8\mu^2\pi^2+7\cos[2\delta_2]+8\cos[2\mu\pi]+\cos[2\delta_2-4\mu\pi] \\ &-8\cos[2\delta_2-2\mu\pi]-4\mu\pi\sin[2\delta_2]+16\mu\pi\sin[2\delta_2-2\mu\pi]\Big\}, \end{aligned} \tag{16}$$

for $i=j$ and

$$\begin{aligned} N^{s2} = N^{a2} &= F[\mu,\nu,\delta_1,\delta_2]+F[\nu,\mu,\delta_1,\delta_3]+F[\nu,-\mu-\nu,\delta_2,\delta_3] \\ &\quad +Q[\mu,\delta_2]+Q[\nu,\delta_3]+Q[-\mu-\nu,\delta_1], \end{aligned} \tag{17}$$

for $i\neq j$, where F and Q are given in equation (A.3) and (A.5) respectively. More details are given appendix A. The propagator can then be written:

$$G(x,y|x',y';t) = \sum_{i=0}^{\infty} \phi^s_{i,i}(x,y)\phi^s_{i,i}(x',y')e^{-t/T_{i,i}} + \sum_{i=0}^{\infty}\sum_{j=i+1}^{\infty}\left[\phi^s_{i,j}(x,y)\phi^s_{i,j}(x',y') + \phi^a_{i,j}(x,y)\phi^a_{i,j}(x',y')\right]e^{-t/T_{i,j}}$$
$$\phi^{s,a}_{i,j} \equiv \frac{T^{s,a}_{i,j}}{N^{s,a}_{i,j}}\,. \tag{18}$$

4 The CPMG amplitude in an equilateral triangle

From equation (4) it is obvious that the antisymmetric modes do not contribute. It actually turns out that only the diagonal modes ($i = j$) give non vanishing contribution to the magnetic signal [1], for further details on this point see Appendix A. From equation (3), (4) and (18) we find :

$$\begin{aligned} M(t) &= e^{-t/T_{2b}}\sum_{i=0}^{\infty}\int\int d\mathbf{r}d\mathbf{r}'\rho(\mathbf{r}')\phi^s_{i,i}(\mathbf{r})\phi^s_{i,i}(\mathbf{r}')e^{-t/T_{i,i}} \\ &= 8e^{-t/T_{2b}}\sum_{i=0}^{\infty}e^{-t/T_{ii}}\int d\mathbf{r}'\rho(\mathbf{r}')T^s_{i,i}(\mathbf{r}') \\ &\times(\cos[\delta_2]-\cos[\delta_2-2\mu\pi]+2\mu\pi\sin[\delta_2]) \\ &\times\Big\{8(1+\mu^2\pi^2)-7\cos[2\delta_2]-8\cos[2\mu\pi]-\cos[2\delta_2-4\mu\pi] \\ &+8\cos[2\delta_2-2\mu\pi]+4\mu\pi\sin[2\delta_2]-16\mu\pi\sin[2\delta_2-2\mu\pi]\Big\}^{-1}. \end{aligned} \tag{19}$$

We need to know the initial excited spin density. We will consider two cases one with uniform spin density, $\rho(\mathbf{r}) = 1/(3\sqrt{3}R^2)$ and one with all the excited spins in the center of the triangle $\rho(\mathbf{r}) = \delta(x-\sqrt{3}R)\delta(y-R)$. For a uniform spin density, the magnetization is:

$$\begin{aligned} M(t) = 12e^{-t/T_{2b}}&\sum_{i=0}^{\infty}\frac{e^{-t/T_{ii}}}{(\mu\pi)^2}(\cos[\delta_2]-\cos[\delta_2-2\mu\pi]+2\mu\pi\sin[\delta_2])^2 \\ &\times\Big\{8(1+\mu^2\pi^2)-7\cos[2\delta_2]-8\cos[2\mu\pi]-\cos[2\delta_2-4\mu\pi] \\ &+8\cos[2\delta_2-2\mu\pi]+4\mu\pi\sin[2\delta_2]-16\mu\pi\sin[2\delta_2-2\mu\pi]\Big\}^{-1}. \end{aligned} \tag{20}$$

And for all the excited spins in the center of the triangle:

[1] This is only the case for the CPMG sequence, for the PFGSE sequence all the modes contribute.

Table 1
Characteristic decay times as a function of surface relaxtivity , pore radius R and diffusion coefficient D in an equilateral triangle. Note that the lowest mode is independent of the diffusion constant in FDL, while the higher modes are independent of the surface relaxtivity

	Fast Diffusion Limit $\tau_D >> \tau_\rho\,(\rho R/D << 1)$	Slow Diffusion Limit $\tau_D << \tau_\rho\,(\rho R/D >> 1)$
$(T_2)_{00}$	$\frac{R}{2\rho}$	$\frac{9R^2}{4D\pi^2}$
$(T_2)_{ii}$	$\frac{9R^2}{4D\pi^2 i^2}$	$\frac{9R^2}{4D\pi^2(1+i)^2}$

$$
\begin{aligned}
M(t) = 24e^{-t/T_{2b}} \sum_{i=0}^{\infty} e^{-t/T_{ii}} \cos[\delta_2 - \frac{2\mu\pi}{3R}] \\
\times(\cos[\delta_2] - \cos[\delta_2 - 2\mu\pi] + 2\mu\pi \sin[\delta_2]) \\
\times\Big\{8(1+\mu^2\pi^2) - 7\cos[2\delta_2] - 8\cos[2\mu\pi] - \cos[2\delta_2 - 4\mu\pi] \\
+8\cos[2\delta_2 - 2\mu\pi] + 4\mu\pi\sin[2\delta_2] - 16\mu\pi\sin[2\delta_2 - 2\mu\pi]\Big\}^{-1}. \quad (21)
\end{aligned}
$$

5 Fast Diffusion and Slow Diffusion Limit

There are two different time scales of interest. The relaxation time which is dependent on the surface relaxivity, $\tau_\rho \sim R/\rho$ and the diffusion time which is dependent on the diffusion constant $\tau_D \sim R^2/D$. If $\tau_D >> \tau_\rho$ then we are in the fast diffusion limit (FDL). On the contrary, if $\tau_\rho >> \tau_D$ then we are in the slow diffusion limit(SDL). In these two limiting cases the eigenvalues and the analytical expression for the magnetic signal simplifies considerably. In the FDL the spins traverse the triangular domain many times before they relax and the magnetic decay is dominated by one mode. By simply replacing tan with its argument in equation (11), we regain the famous result by Brownstein and Tarr[6], by direct calculation:

$$\frac{1}{T_2} = \rho\frac{2}{R} = \rho\frac{S}{V}\,. \quad (22)$$

We write the magnetic signal from the equilateral triangle as $M(t) = \sum_i^\infty I_{ii}\exp(-t/T_{ii})$, the coefficients and eigenvalues are summarized in the table 1 and 2. As seen from table 2, the FDL is dominated by one mode and hence a single decay time. In figure 2 we have plotted the eigenvalues as a function of γ.

As seen from figure 2 and 3 the eigenvalues, compared to the intensities, first deviate from the FDL value for increasing γ. This means that the magnetic decay is still mono exponential, but the simple relation $T_2^{-1} = \rho S/V$ is vi-

Table 2
The intensities in the fast and slow diffusion limit. Note that the sum of the intensities add up to one as they should, $\sum_{i=0}^{\infty} 1/(1+i)^2 = \pi^2/6$ and $\sum_{i=0}^{\infty} \sin[2(1+i)\pi/3]/(1+i) = \pi/6$

	Fast Diffusion Limit $\tau_D >> \tau_\rho\,(\rho R/D << 1)$	Slow Diffusion Limit $\tau_D << \tau_\rho\,(\rho R/D >> 1)$
I_{ii} uniform density	$\delta_{i,0}$	$\frac{6}{(1+i)^2\pi^2}$
I_{ii} delta density	$\delta_{i,0}$	$\frac{6\sin[2(1+i)\pi/3]}{(1+i)\pi}$

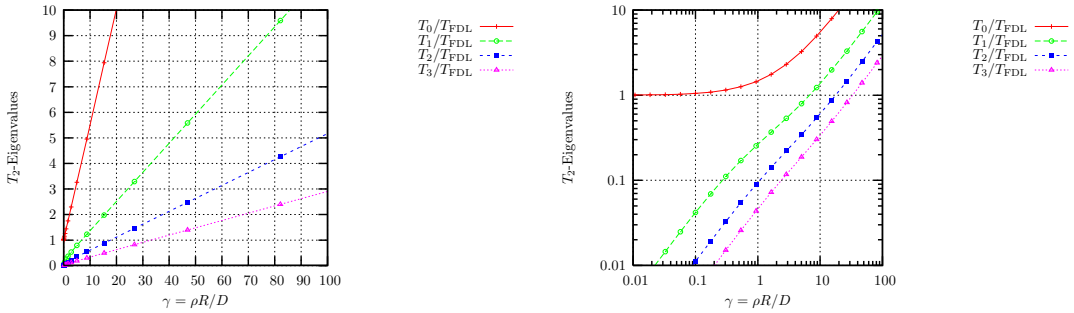

Fig. 2. Left: The eigenvalues as a function of γ, $T_{\rm FDL} = r/(2\rho)$. Right: same as left but log-log plot. For $\gamma = 0.1$ there is a 10% deviation and at $\gamma = 0.4$ there is a 20% deviation from the FDL.

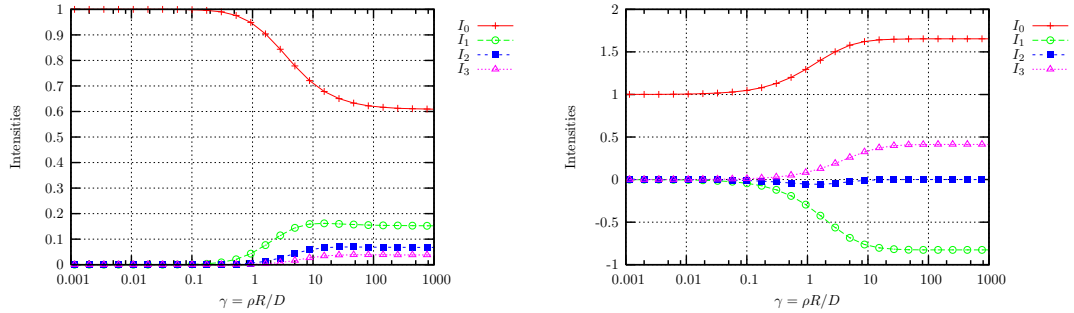

Fig. 3. Left: the first four intensities for uniform initial spin density. Right: the first four modes for all spins initially at the center of the triangle. Note that the asymptotic limit for the intensities are $I_0 = 0.61, 1.65$, $I_1 = 0.15, -0.83$, $I_2 = 0.07, 0$ and $I_3 = 0.04, 0.41$ for the uniform and delta densities respectively.

olated. The deviation in the intensities from the FDL happens faster in the case where all the spins start in the center. This should be no surprise as the spins must transverse a larger area, in this case, before they relax.

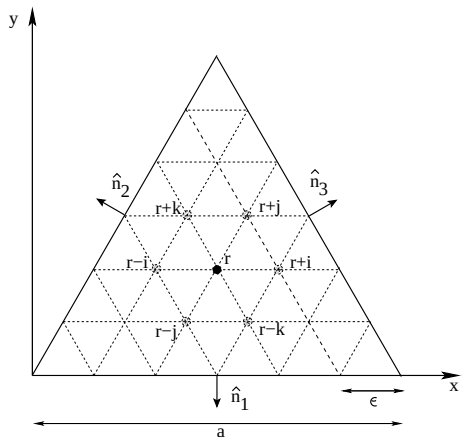

Fig. 4. Grid for random walk simulation, lattice spacing ϵ and side length a, unit outward normal vectors $\hat{\mathbf{n}}_{1,2,3}$,

6 Numerical Algorithm - Random Walk

One way of numerically studying the NMR signal from a pore is by random walk simulations[22]. For random walk simulation in an equilateral triangle we choose a hexagonal grid, see figure 4. A random walker is placed at random at a lattice point in the equilateral triangle. The number of random walkers at an interior point r (see figure 4) when the clock advance one step τ is then given by :

$$\begin{aligned} M(\boldsymbol{r},t+\tau)-M(\boldsymbol{r},t) = \frac{1}{6}\Big[&M(\boldsymbol{r}+\epsilon\hat{\boldsymbol{i}},t)-M(\boldsymbol{r},t)+M(\boldsymbol{r}-\epsilon\hat{\boldsymbol{i}},t)-M(\boldsymbol{r},t) \\ &+\Big\{\text{id. with } (\hat{\boldsymbol{i}}\to\hat{\boldsymbol{j}})\Big\}+\Big\{\text{id. with } (\hat{\boldsymbol{i}}\to\hat{\boldsymbol{k}})\Big\}\Big] \\ &-\kappa M(\boldsymbol{r},t) \end{aligned} \tag{23}$$

The probability for a random walker to take a step in each direction is 1/6, the probability for a random walker to die during the timestep τ is κ. Dividing by τ, we find:

$$\begin{aligned} \frac{M(\boldsymbol{r},t+\tau)-M(\boldsymbol{r},t)}{\tau} = \frac{\epsilon^2}{6\tau}\Bigg[&\frac{M(\boldsymbol{r}+\epsilon\hat{\boldsymbol{i}},t)-2M(\boldsymbol{r},t)+M(\boldsymbol{r}-\epsilon\hat{\boldsymbol{i}},t)}{\epsilon^2} \\ &+\Big\{\text{id. with } (\hat{\boldsymbol{i}}\to\hat{\boldsymbol{j}})\Big\}+\Big\{\text{id. with } (\hat{\boldsymbol{i}}\to\hat{\boldsymbol{k}})\Big\}\Big] \\ &-\frac{\kappa}{\tau}M(\boldsymbol{r},t) \end{aligned} \tag{24}$$

The lattice spacing is given by ϵ. Taking the limit $\tau\to 0$, $\epsilon\to 0$, $\kappa\to 0$:

$$\frac{\partial M}{\partial t} = \frac{\epsilon^2}{6\tau}\left[\frac{\partial^2 M}{\partial i^2}+\frac{\partial^2 M}{\partial j^2}+\frac{\partial^2 M}{\partial k^2}\right]-\frac{\kappa}{\tau}M(\boldsymbol{r},t)\,. \tag{25}$$

Changing from lattice coordinates to Cartesian coordinates:

$$\frac{\partial^2}{\partial i^2}+\frac{\partial^2}{\partial j^2}+\frac{\partial^2}{\partial k^2}=\frac{3}{2}\left(\frac{\partial^2}{\partial x^2}+\frac{\partial^2}{\partial y^2}\right), \tag{26}$$

we finally arrive at :

$$\frac{\partial M}{\partial t}=D\nabla^2 M-\frac{M}{T_{2b}}, \quad \text{where} \tag{27}$$

$$D=\frac{\epsilon^2}{4\tau} \qquad \text{and} \qquad \frac{1}{T_{2b}}=\frac{\kappa}{\tau}\,. \tag{28}$$

This is the same equation as (1). Consider the surface normal to the $\hat{\mathbf{n}}_3$-vector (in figure 4), at a lattice point at the boundary surface give the following equation:

$$\begin{aligned}\epsilon\frac{M(\boldsymbol{r},t+\tau)-M(\boldsymbol{r},t)}{\tau}=&\frac{2}{3}\epsilon\frac{\epsilon^2}{4\tau}\left[\frac{M(\boldsymbol{r}+\epsilon\hat{\boldsymbol{k}},t)-2M(\boldsymbol{r},t)+M(\boldsymbol{r}-\epsilon\hat{\boldsymbol{k}},t)}{\epsilon^2}\right]\\&+\frac{2}{3}\frac{\epsilon^2}{4\tau}\frac{M(\boldsymbol{r}-\epsilon\hat{\boldsymbol{i}},t)-M(\boldsymbol{r},t)}{\epsilon}\\&+\frac{2}{3}\frac{\epsilon^2}{4\tau}\frac{M(\boldsymbol{r}-\epsilon\hat{\boldsymbol{j}},t)-M(\boldsymbol{r},t)}{\epsilon}\\&-\frac{1}{3}\frac{\zeta\epsilon}{\tau}M(\boldsymbol{r},t)\\&-\epsilon\frac{\kappa}{\tau}M(\boldsymbol{r},t)\end{aligned} \tag{29}$$

We have assumed that the walkers have a probability ζ of being killed when hitting the wall. If a walker is not killed it is assumed to return to the interior point in the same timestep. In the limit $\tau\to 0$, $\epsilon\to 0$, the fractions involving M are recognized to approach $\partial M/\partial t$, $\partial^2 M/\partial\epsilon^2$, $-\partial M/\partial i$ and $-\partial M/\partial j$, respectively. Using the following relation:

$$\frac{\partial}{\partial i}+\frac{\partial}{\partial j}=\sqrt{3}\;\hat{\mathbf{n}}_3\cdot\nabla \tag{30}$$

and as the LHS and the first term on the RHS in equation (29) are of higher order in ϵ, they can be neglected compared to the others, hence :

$$D\mathbf{n}_3\cdot\nabla M+\rho M=0 \qquad \text{and} \qquad \rho=\frac{1}{2\sqrt{3}}\frac{\zeta\epsilon}{\tau}\,. \tag{31}$$

By symmetry the other boundary sides give the same answer and we then regain equation (2).

Using the fact that number of lattice points from corner to corner along an edge is

$$N = 1 + a/\epsilon\,, \tag{32}$$

from equation (28) and (31) we find the following important relation:

$$\gamma = \frac{\rho r}{D} = \frac{1}{3}(N-1)\zeta \tag{33}$$

For a given γ the probability for a random walker to die when it hits the wall can be calculated from equation(33).

The magnetic signal can then be calculated numerically by placing a number of random walkers inside the equilateral triangular domain. For uniform initially spin density the walkers are placed at random and for the delta density all the walkers start in the center of the triangle. At each timestep the walkers take one step of length ϵ and dies with a probability κ. If the walkers hits the wall it dies with probability ζ. The magnetic signal will then be proportional to the number of walkers at each timestep τ. The lattice spacing and time is related to the physical length and time by using equation (28).

6.1 The relative importance of relaxation types

Let θ denote the ratio of bulk relaxation and boundary relaxation rates. In the fast diffusion limit, with a comparatively flat distribution of walkers, θ can be estimated by combining the ratio of bulk lattice points[2] $(N(N+1)/2)$ to boundary lattice points $(3(N-1))$ with the appropriate ratio of relaxation probabilities (a boundary walker will suffer relaxation with probability $\zeta/3$ on this lattice except in the very corner positions, where the probability is $2\zeta/3$):

$$\begin{aligned} \theta \quad &= \quad \frac{N}{2}\frac{1+1/N}{(1-1/N)^2}\frac{\kappa}{\zeta} = \frac{1}{4\sqrt{3}}\frac{a}{\rho T_{2b}}\frac{N^2(N+1)}{(N-1)^3} \\ &\xrightarrow[\epsilon\to 0]{} \quad \frac{1}{4\sqrt{3}}\frac{a}{\rho T_{2b}} = \frac{1}{6}\frac{\frac{a^2}{4D}}{\gamma T_{2b}} \end{aligned} \tag{34}$$

As follows from inspection of equation (27) and (31), and implicitly stated by Brownstein and Tarr[5,6] the solutions for the average magnetization M will be three-parameter functions. In addition to γ and θ, one of the intrinsic time scales, τ_D for diffusion and τ_ρ for relaxation at the boundary, respectively, may

[2] *The boundary points counted among them here, since both ζ and κ small in the limit $N \to \infty$ ($\epsilon \to 0$). If not, $(N-2)(N-3)/2$ to be used; anyway no difference in the limit $\epsilon \to 0$.*

be chosen as a parameter:

$$\tau_D = \frac{a^2}{4D} = 1.25\,\mathrm{s} \times \left(\frac{a}{0.1\,\mathrm{mm}}\right)^2 \left(\frac{2 \times 10^{-5}\,\mathrm{cm}^2/\mathrm{s}}{D}\right) \tag{35}$$

$$\tau_\rho = \frac{a^2}{4D}/\gamma = 2\sqrt{3}\frac{a}{\rho} = 17.32\,\mathrm{s} \times \left(\frac{a}{0.1\,\mathrm{mm}}\right) \left(\frac{5\,\mu\mathrm{m}/\mathrm{s}}{\rho}\right) \tag{36}$$

One such set of parameters may thus be

$$\{\gamma, \frac{a^2}{4D}, \theta\}$$

From equation (34) it follows that, physically, θ depends on the bulk sink strength density measured in units of the inverse time scale for relaxation at the boundary.

6.2 Scaling in random walk simulations

Eliminating ϵ between equation (28) and equation (32) gives a relation between the intrinsic time scale for diffusion and the time step length in a simulation with a given N value:

$$\tau(N-1)^2 = \frac{a^2}{4D} \tag{37}$$

If, for given γ and θ values, the average magnetization is plotted not against the actual time t or the integer time step counter t/τ but in units of the intrinsic time scale, viz., a plot against

$$\frac{t}{\tau(N-1)^2}$$

then the results for various $\{N, \zeta\}$ consistent with the given γ value should be expected to plot on top of each other, provided inaccuracies due to finite N values are unimportant. This follows since $t/\tau \propto (N-1)^2$, where N is not a physical parameter but an artificial one determined by the simulation conditions. Technically, there would thus be a scaling property in the limit $N \to \infty$, in that the magnetization should depend only on a certain algebraic combination of simulation parameters.

The predicted scaling has been checked numerically for several γ values, using $\theta = 0$ (no bulk relaxation), and has indeed been found to hold. (The origins and magnitude of deviations from exact scaling will be discussed below.) Its practical value is that for a given simulation, one may choose that set of values for $\{N, \zeta\}$ which gives an optimally acceptable combination of accuracy and computing time requirements.

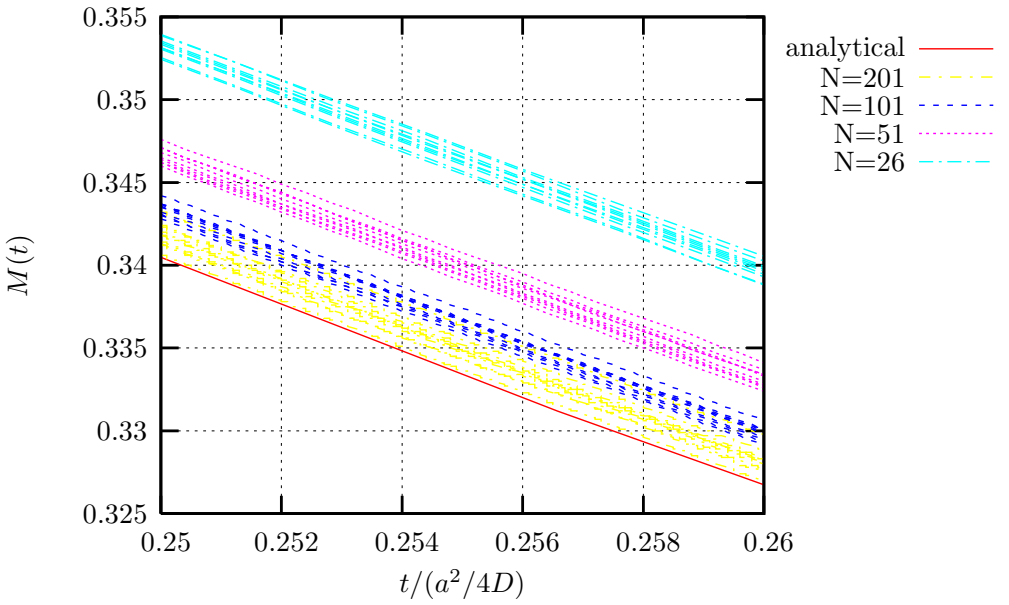

Fig. 5. (N, ζ)-dependency for $\gamma = 1$, 10^6 walkers (Mersenne Twister). Note that as N increases the numerical solution moves towards the analytical solution

6.3 Sources and estimates of simulation inaccuracy

Figure 5 shows the results of simulations of the average magnetization M for $\gamma = 1$, in an interval of scaled time t/τ_D. The N values 26, 51, 101 and 201 were used; for each, 10 simulations with different random number generator seeds have been plotted, with $N_w = 10^6$ random walkers released on the lattice in each simulation. The lowermost line shows the analytical solution in the same interval, plotted as the sum of 50 modes. The 'Mersenne Twister' generator[23] was used in this plot as random number generator, but also runs with single-precision versions of ran2 and ran3[24] were made. The simulations organize themselves in bands corresponding to the four N values used, with N increasing from above (the bands for $N = 101$ and $N = 201$ partially merging).

Various sources of error in the simulations can be discerned:

- Random:
  - Small fluctuations in the curves increase with increasing N, for the same number of random walkers.
  - Generator seed / number of walkers: With each curve showing an average over $N_w = 10^6$ walkers, for each N value there is still a seed-dependent spread within a band of the order of 0.7 %.
  - Truncation errors do not give important random effects in these simulations; curves for a single-precision ran3 (not shown) have about the same variance as those shown here.

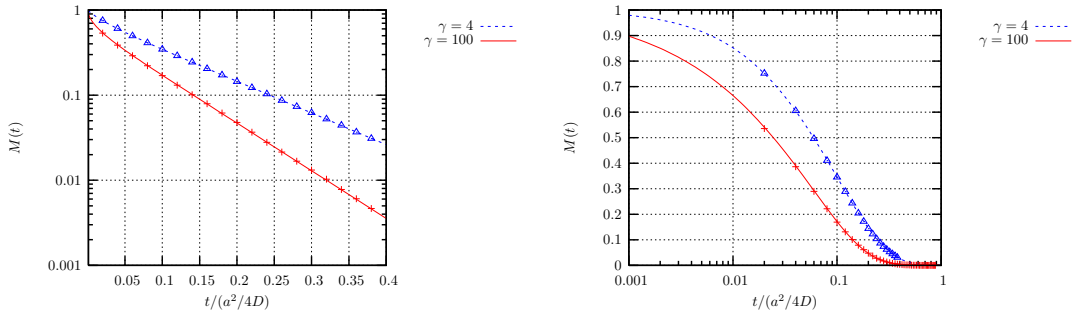

Fig. 6. Left:Comparison of random walk simulation (points) and analytical solution (line) for $\gamma = 4$ and 100. $N = 501$ and 10^6 random walkers. The initial spin density is uniform. Right: Same as left but log scale on the x-axis instead of the y-axis.

- Systematic:
  - Finite ϵ effects: Since $\epsilon \propto 1/(N-1)$, choosing N too small makes the order ϵ terms in equation (29) increase in importance, thus violating equation (31) in addition to introducing inaccuracies in the representation of the derivatives in equation (27) and (31). The simulation results averaged over seed values show a deviation from the analytical solution as a monotonous function of N, of order 1 % for $N = 101$ and rapidly increasing as N decreases. (Technically, these N-dependent systematic deviations may be considered a 'scaling violation'.)
  - Truncation errors: For $N = 26$ the results for ran3 (not shown) and for Mersenne Twister are very close, but for increasing N the average difference between the bands becomes larger for ran3 than for Mersenne Twister, so that for large N the bands actually make an 'undershoot' (not shown) of the analytical result. Such effects may arise from truncation when a random generator is used to make a choice with a given probability.

The level of accuracy may vary with γ and with the range of scaled time used. For the values treated above, we conclude that $N \gtrsim 200$ and $N_w \gtrsim 10^6$ should be used to obtain an accuracy in one given run of order 1 % or better.

In figure 6 and 7 we have compared numerical and analytical results. There is clearly a very good match. The largest deviation between numerical and analytical results are for long times. This is natural as the number of walkers is low and the statistic is poorer.Note that if one extrapolate the straight line for high γ values in figure 6 (left) and 7 (left), it crosses the y-axis at $6/\pi^2$ and $6/\pi$. We have also made some comparison with $\theta \neq 0$, i.e. with bulk relaxation (see equation (34)). In figure 8, we have plotted results for $\theta = 0.1$, 1. $\theta = 0.1, 1$ corresponds to a bulk relaxation of 1.7, 0.17 s respectively.

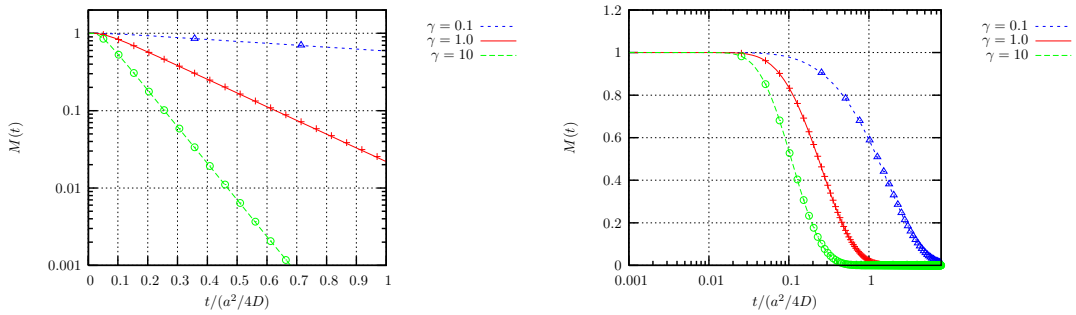

Fig. 7. Left:Comparison of random walk simulation (points) and analytical solution (line) for $\gamma = 0.1, 1$ and 10. The initial spin density is a delta density. $N = 501$ and 10^6 random walkers. Right: Same as left but log scale on the x-axis instead of the y-axis.

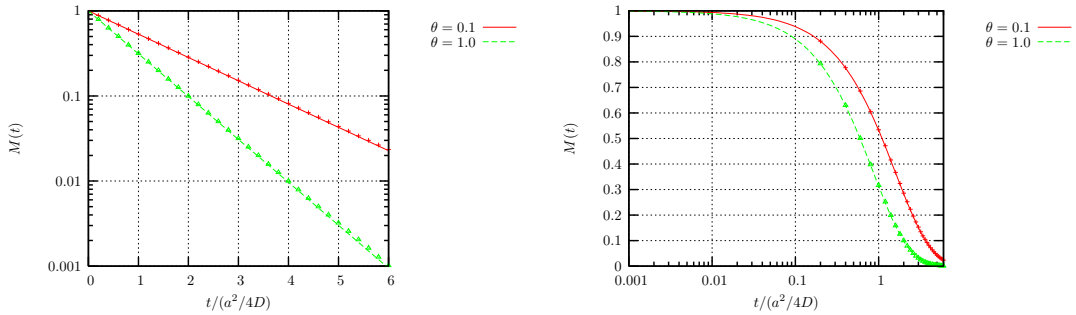

Fig. 8. Left:Comparison of random walk simulation (points) and analytical solution (line) for $\theta = 0.1, 1$, $\gamma = 1$. Uniform initially spin density, $N = 201$ and 10^6 random walkers. Right: Same as left but log scale on the x-axis instead of the y-axis.

7 Conclusion

We have presented an analytical solution for the magnetic signal from an equilateral triangular pore, with surface relaxation. To our knowledge this solution has not been presented before. This solution will be used in theoretical studies of single- and two-phase NMR response from equilateral triangles, which can be used as basic building blocks for pore scale models. This solution is also very important when interpreting experiments done at equilateral triangular tubes, which is in progress at our group.

We have considered two initial conditions. In the first case the spin density is uniform and in the second case all the excited spins are concentrated in the center of the triangle. In both cases there is an excellent agreement between theory and the random walk simulations.

In a forthcoming paper we will present results for the PFGSE sequence, the single-phase result can be calculated from the Green's function presented in this paper. Two-phase results for any value of γ must in general be solved by

a random walk algorithm, except for the limit $\gamma \to 0$ where analytical results can be found. The analytical result will then serve to calibrate the numerical random walk algorithms for two-phase.

Acknowledgments
The authors acknowledge ConocoPhillips and the Ekofisk Coventurers, including TOTAL, ENI, Hydro, Statoil and Petoro, for financing the work and for the permission to publish this paper from the research center COREC.

A Normalization and eigenfunction integral over the triangular domain

$$N^{s,a2} = \int_0^{3r} \int_{y/\sqrt{3}}^{-y/\sqrt{3}+2\sqrt{3}r} T_{s,a}(x,y) T_{s,a}(x,y) \tag{A.1}$$

in an obvious notation, the subscript i, j has been suppressed. After a rather lengthy manipulation, the result can be written:

$$\begin{aligned} N_{s,a}^2 = & F[\mu,\nu,\delta_1,\delta_2] \pm G[\mu,\nu,\delta_1,\delta_2] + F[\nu,\mu,\delta_1,\delta_3] \pm G[\nu,\mu,\delta_1,\delta_3] \\ & + F[\nu,-\mu-\nu,\delta_2,\delta_3] \pm G[\nu,-\mu-\nu,\delta_2,\delta_3] \\ & + Q[\mu,\delta_2] \pm P[\mu,\nu,\delta_2] + Q[\nu,\delta_3] \pm P[\nu,\mu,\delta_3] \\ & + Q[-\mu-\nu,\delta_1] \pm P[-\nu-\mu,\mu,\delta_1]\,, \end{aligned} \tag{A.2}$$

the lower sign is for the anti symmetric mode and the upper sign for the symmetric modes and:

$$\begin{aligned} F[\mu,\nu,\delta_1,\delta_2] = & -\frac{3\sqrt{3}r^2}{4\mu\nu^2(\mu+\nu)\pi^2} \{\nu\cos[\delta_1-\delta_2](\nu+\mu\cos[2(\mu+\nu)\pi]) \\ & + (\mu+\nu)(-\nu\cos[\delta_1-\delta_2+2\mu\pi] \\ & - \mu\cos[\delta_1+\delta_2] + \mu\cos[\delta_1+\delta_2+2\nu\pi] + 2\mu\nu\pi\sin[\delta_1+\delta_2]) \\ & - \sin[\delta_1-\delta_2]\sin[2(\mu+\nu)\pi]\} \end{aligned} \tag{A.3}$$

$$G[\mu,\nu,\delta_1,\delta_2] = -\frac{27\sqrt{3}r^2}{8(2\mu+\nu)\pi^2}((\frac{1}{\mu^2+\mu\nu-2\nu^2}$$
$$(2(-(2\mu+\nu)\cos[\delta_1+\delta_2]+(\mu+2\nu)\cos[\delta_1+\delta_2+\frac{2}{3}(-\mu+\nu)\pi]$$
$$+(\mu-\nu)\cos[\delta_1+\delta_2+\frac{2}{3}(\mu+2\nu)\pi]))$$
$$-\frac{4\cos[\delta_1-\delta_2+\frac{2}{3}(2\mu+\nu)\pi]\sin[\frac{1}{3}(2\mu+\nu)\pi]^2}{2\mu+\nu})) \qquad (A.4)$$

$$Q[\mu,\delta_2] = \frac{3\sqrt{3}r^2}{8\mu^2\pi^2}(\cos[2(\delta_2-\mu\pi)]-\cos[2\delta_2]$$
$$+2\mu\pi(\mu\pi-\sin[2(\delta_2-\mu\pi)])) \qquad (A.5)$$

$$P[\mu,\nu,\delta_2] = -\frac{27\sqrt{3}r^2}{32(\mu-\nu)(2\mu+\nu)(\mu+2\nu)^2\pi^2}$$
$$((\mu+2\nu)((\mu+2\nu)\cos[2\delta_2]-(2\mu+\nu)\cos[2\delta_2+\frac{4}{3}(-\mu+\nu)\pi]$$
$$+\cos[2\delta_2-\frac{4}{3}(2\mu+\nu)\pi])-8(\mu-\nu)(2\mu+\nu)\sin[\frac{1}{3}(\mu+2\nu)\pi]^2)) \qquad (A.6)$$

As a partial check on the calculation, we may consider the diagonal elements. In this case equation (14) is valid and after a short calculation one finds:

$$N_{ii}^{s\,2} = -\frac{9\sqrt{3}r^2}{16\mu^2\pi^2}\Big\{-8-8\mu^2\pi^2+7\cos[2\delta_2]+8\cos[2\mu\pi]+\cos[2\delta_2-4\mu\pi]$$
$$-8\cos[2\delta_2-2\mu\pi]-4\mu\pi\sin[2\delta_2]+16\mu\pi\sin[2\delta_2-2\mu\pi]\Big\} \qquad (A.7)$$

Using $\delta_2 \to \delta_3$, $\mu \to \nu$ and $\delta_1 \to \delta_2 - 2\pi\mu + 2i\pi$, we find from equation (A.3-A.6)

$$G[\nu,\mu,\delta_1,\delta_3] \to G[\mu,\nu,\delta_1,\delta_2] \to F[\nu,\mu,\delta_1,\delta_3] \to F[\mu,\nu,\delta_1,\delta_2]$$
$$\to \frac{3\sqrt{3}r^2\cos[\delta_2-\mu\pi]}{2\mu^2\pi^2}$$
$$\times\Big(\cos[\delta_2-\mu\pi]-\cos[\delta_2+\mu\pi]-2\mu\pi\sin[\delta_2-\mu\pi]\Big) \tag{A.8}$$
$$P[\nu,\mu,\delta_3] \to P[\mu,\nu,\delta_2] \to \frac{1}{2}F[\nu,-\mu-\nu,\delta_2,\delta_3]$$
$$\to \frac{3\sqrt{3}r^2}{8\mu^2\pi^2}$$
$$\times\Big(1+\cos[2\delta_2]-\frac{1}{4}\cos[2\mu\pi]-\frac{1}{4}\cos[2\delta_2-4\mu\pi]$$
$$+\mu\pi\sin[2\delta_2]\Big) \tag{A.9}$$
$$Q[\nu,\delta_3] \to Q[\mu,\delta_2] \to +\frac{1}{2}G[\nu,-\mu-\nu,\delta_2,\delta_3]$$
$$\to -\frac{3\sqrt{3}r^2}{8\mu^2\mu\pi^2}$$
$$\times\Big(\cos[2\delta_2]-\cos[2\delta_2-2\mu\pi]-2\mu\pi(\mu\pi-\sin[2\delta_2-2\mu\pi])\Big) \tag{A.10}$$
$$P[-\mu-\nu,\mu,\delta_1] \to Q[-\mu-\nu,\delta_1]$$
$$\to \frac{3\sqrt{3}r^2}{32\mu^2\pi^2}$$
$$\times\Big(\cos[2\delta_2]-\cos[2\delta_2-4\mu\pi]+4\mu\pi(2\mu\pi+\sin[2\delta_2])\Big) \tag{A.11}$$

Summing these equations, $N^s_{ii} = 4\times(\,(A.8)+(A.9)+(A.10)+(A.11)\,)$ we find that N^s_{ii} is given by equation (A.7) and $N^a_{ii}=0$. Actually it turns out that when $i\neq j$, we have :

$$N^{s2} = N^{a2} = F[\mu,\nu,\delta_1,\delta_2]+F[\nu,\mu,\delta_1,\delta_3]+F[\nu,-\mu-\nu,\delta_2,\delta_3]$$
$$+Q[\mu,\delta_2]+Q[\nu,\delta_3]+Q[-\mu-\nu,\delta_1]\,, \tag{A.12}$$

The last equation is verified by solving the boundary conditions (11) numerically for different values of $\gamma=\rho r/D$.

Integrating the symmetric modes over the equilateral triangular domain, we find:

$$
\begin{aligned}
A_{\mathrm{CPMG}} &= \int_0^{3r}\int_{y\sqrt{3}}^{-y\sqrt{3}+2\sqrt{3}r} dxdyT_s(x,y) \\
&= -\frac{27\sqrt{3}r^2}{2\pi^2(\mu-\nu)(2\mu+\nu)(\mu+2\nu)} \\
&\times\Big\{(\mu-\nu)\cos[\delta_1]+(\mu+2\nu)\cos[\delta_2]-(2\mu+\nu)\cos[\delta_3] \\
&+(\mu+2\nu)\cos[\delta_3+\frac{2\pi}{3}(\mu-\nu)]-(2\mu+\nu)\cos[\delta_2+\frac{2\pi}{3}(-\mu+\nu)] \\
&+(\mu-\nu)\cos[\delta_2-\frac{2\pi}{3}(\mu+\nu)]+(\mu+2\nu)\cos[\delta_1+\frac{2\pi}{3}(2\mu+\nu)] \\
&+(\mu-\nu)\cos[\delta_3-\frac{2\pi}{3}(\mu+2\nu\pi)]-(2\mu+\nu)\cos[\delta_1+\frac{2\pi}{3}(\mu+2\nu)]\Big\} \qquad \text{(A.13)}
\end{aligned}
$$

From equation (12), we find:

$$
\mu = -\frac{\delta_1-2\delta_2+\delta_3}{2\pi}+i \qquad \nu = -\frac{\delta_1-2\delta_3+\delta_2}{2\pi}-j \qquad \text{(A.14)}
$$

We need to consider two cases separately, $j=i$, $j=i \mod 3 (i\neq j)$. For $j=i$ we have in addition $\delta_3=\delta_2$ $(\mu=\nu)$. We then find:

$$
A^{i=j}_{\mathrm{CPMG}} = \frac{9\sqrt{3}r^2}{2\mu^2\pi^2}\{\cos[\delta_2]-\cos[\delta_2+2i\pi-2\mu\pi]+2\mu\pi\sin[\delta_2]\} \qquad \text{(A.15)}
$$

For $j=i \mod 3 (j\neq i)$, we write $j=i+3k$, $k=1,2,\ldots$:

$$
\begin{aligned}
A^{k}_{\mathrm{CPMG}} = & \frac{18\sqrt{3}r^2}{(\delta_2-\delta_3-2k\pi)(-\delta_1+\delta_2+2(i+k)\pi)(-\delta_1+\delta_3+2(i+2k)\pi)} \\
&\times\{(-\delta_2+\delta_3+2k\pi)\cos[\delta_1]+(\delta_1-\delta_3-2(i+2k)\pi)\cos[\delta_2] \\
&+(-\delta_1+\delta_2+2(i+k)\pi)\cos[\delta_3]\} \qquad \text{(A.16)}
\end{aligned}
$$

For the other cases, we find $A_{\mathrm{CPMG}}=0$. Using the constraints imposed by the boundary conditions (11) it turns out that $A^k_{\mathrm{CPMG}}=0$, this has been verified numerically by solving equation (11) for different values of $\gamma=\rho r/D$. We are then left with equation (A.15) as the final result for the CPMG sequence.

References

[1] R. Freedmann, N. Heaton, M. Flaum, G. Hirasaki, C. Flaum, M. Hurlimann, Wettability, Saturation, and Viscosity Using the Magnetic Resonance Fluid Characterizing Method and New Diffusion-Editing Pulse Sequences, *SPE***77397**,2002 SPE Annual Technical Conference and Ehibition, San Antonio, Sep 29-Oct 2.

[2] N. Heaton, R. Freedman, C. Karmonik, R. Taherian, K. Walter, L. Depavia, Application of a New-Generation NMR Wireline Logging Tool, *SPE* **77400**, 2002 SPE Annual Technical Conference and Exhibition, San Antonio, Sep 29 - Oct 2.

[3] M. Hürlimann, L. Venkataramanan, C. Flaum, P. Speier,C. Karmonik, R. Freedman, N. Heaton, Diffusion-Editing: New NMR Measurement of Saturation and Pore Geometry, the 2002 SPWLA Annual Logging Symposium, Houston, June 2-5.

[4] M. Hürliman, L. Venkataramanan, Quantitative Measurement of Two-Dimensional Distribution Functions of Diffusion and Relaxation in Grossly Inhomogeneous Fields, *J. Mag. Reson.* **157**, 31-42, (2002)

[5] K. Brownstein, C. Tarr,Spin-Lattice Relaxation in a System Governed by Diffusion, *J. Mag. Reson* **26**,(1977), 17-24

[6] K. Brownstein, C. Tarr, Importance of Classical Diffusion in NMR Studies of Water in Biological Cells, *Phys. Rev.* **A**, 19 (1979), 2446-2453.

[7] Q. Zhang, C. Huang, G. Hirasaki, Interpretation of Wettability in Sandstones With NMR Analysis, *Petrophysics* **41**, 3 (2000), 223-233.

[8] C. Radke, A. Kovscek, H. Wong,A Pore-Level Scenario for the Development of Mixed Wettability , *SPE* **24880**, the 1992 Annual Technical Conference and Exhibition of the Society of Petroleum Engineers, Washington DC, Oct. 4-7.

[9] G. Mason, N. Morrow, Capillary behavior of a perfectly wetting liquid in irregular triangular tubes, *J. Coll. Int. Sci.* **141** (1991), 262-274.

[10] N. Morrow, G. Mason, Recovery of Oil by Spontaneous Imbibition, *Curr Opin Coll Int Sci* **6** (2001) 321.

[11] M. Jackson, P. Valvatne,M. Blunt,Prediction of wettability variation and its impact on waterflooding using pore- to reservoir-scale simulation, *SPE* **77543**, 2002 SPE Annual Technical Conference and Exhibition, San Antonio, Sep 29 - Oct 2.

M. Piri, Martin. Blunt,Pore-scale modeling of three-phase flow in mixed-wet system, *SPE* **77726**, 2002 SPE Annual Technical Conference and Exhibition, San Antonio, Sep 29 - Oct 2.

M. Hui, M. Blunt, Effects of Wettability on Three-Phase Flow in Porous Media, *J. Phys. Chem.* **B** (2000), 104, 3833-3845

[12] M. van Dijke, K. Sorbie, Three-phase capillary entry conditions in pores of noncircular cross-section, *J. Colloid Interface Sci* **260** (2003) 385-397

[13] J. Helland, S. Skjæveland, Physically-Based Capillary Pressure Correlation for Mixed Wet Reservoirs From a Bundle of Tubes Model, *SPE* **89428**, 2004 SPE/DOE Fourteenth Symposium on Improved Oil Recovery, Tulsa, Apr 17-21.

J. Helland, M. Skjæveland, Three-phase mixed-wet capillary pressure curves from a bundle-of-triangular-tubes model, The 8th International Symposium on Reservoir Wettability, Houston, May 16-18, 2004.

[14] S. Al-Mahrooqi, C. Grattoni, A. Muggeridge, R. Zimmerman, X. Jing, Pore-Scale Modelling of NMR Relaxation for the Characterization of Wettability, paper presented at the 8th International Symposium on Reservoir Wettability, Houston, May 16-18, 2004.

[15] H. Carr, E. Purcell, Effects of diffusion on free precession in NMR experiments, *Phys. Rev.* **94** (1954) 630

S. Meiboom, D. Gill, Compensation for pulse imperfections in Carr-Purcell NMR experiments, *Rev. Sci. Instrum.* **29** (1958) 688

[16] P. Callaghan, "Principles of Nuclear Magnetic Resonance Microscopy", Oxford Univ. Press, Oxford, 1991

[17] W. Price, Pulsed-field gradient nuclear magnetic resonance as a tool for studying translational diffusion: Part 1. Basic theory.*Concepts Magn. Reson.* **9** (1997), 299-336.

[18] W. Price, Pulsed-field gradient nuclear magnetic resonance as a tool for studying translational diffusion: Part II. Experimental aspects. *Concepts Magn. Reson.* **10** (1998), 197-237.

[19] B. Mccartin,Eigenstructure of the Equilateral Triangle, Part II: The Neuman Problem Triangle, *Math. Probl. Eng.* **8** (2002) 517-539

[20] B. Mccartin, Eigenstructure of the Equilateral Triangle, Part I: The Dirichlet Problem, *SIAM Review* **45** (2003) 267-287

[21] B. Mccartin,Eigenstructure of the Equilateral Triangle. Part III. The Robin Problem, *IJMMS* **16** (2004) 807-825

[22] D. Wilkinson, D. Johnson, L. Schwartz, Nuclear magnetic relaxation in porous media: The role of the mean lifetime $\tau(\rho, D)$, *Phys Rev B* **44**, (1991) 4960-4973

P. Mitra, P. Sen, L. Schwartz, Short time behavior of the diffusion coefficient as a geometrical probe of porous media pore geometries, *Phys. Rev. B* **47** (1993) 8565-8574

K. Mendelson,Continuum and random-walk models of magnetic relaxation in porous media, *Phys. Rev. B* **47** (1993) 1081-1083

K. Mendelson, Percolation model of nuclear magnetic relaxation in porous media , *Phys. Rev. B* **41** (1990) 562-567

D. Bergman, K. Dunn, L. Schwartz, P. Mitra, Self-diffusion in a periodic porous medium: A comparison of different approaches, *Phys. Rev. E* **51** (1990) 3393-3400

E. Toumelin, C. Torres-Verdn, S. Chen, Modeling of Multiple Echo-Time NMR Measurements for Complex Pore Geometries and Multiphase Saturations, *SPE* **85635**, 2002 SPE Annual Technical Conference and Exhibition, San Antonio, Sep 29 - Oct 2.

[23] M. Matsumoto, T. Nishimura, Mersenne Twister: A 623-dimensionally equidistributed uniform pseudorandom number generator, *ACM Trans. Mod. and Comp. Sim.* **8** (1998) 3-30

M. Matsumoto, T. Nishimura, Dynamic Creation of Pseudorandom Number Generators, Monte Carlo and Quasi-Monte Carlo Methods 1998, Springer, 2000, 56-69

[24] W. Press et al., Numerical Recipes in C (Cambridge, 1992).